Lifescience Global

Journal of Coating Science and Technology
http://www.lifescienceglobal.com/journals/journal-of-coating-science-and-technology

Determination of Thermal Barrier Coatings Layers Optimum Thickness via PSO-SA Hybrid Optimization Method concerning Thermal Stress

Ali Ghaseminezhad Koushali[1], M. Nazari[2] and Masoud Roudneshin[3,*]

[1]*Faculty of Mechanical & Energy Engineering, Shahid Beheshti University, A.C.,* 1983969411*, Tehran, Iran*

[2]*Center for Postgraduate Studies, Aeronautical University of Science and Technology, Sought Mehrabad, Shamshiri st., 13846-73411 Tehran, Iran*

[3]*Department of Electrical and Computer Engineering, University of Montreal, Concordia, Canada*

Abstract: Turbine entry temperature of turbo-engines has been increased to improve proficiency. Consequently, protecting the hot section elements experiencing aggressive service conditions necessitates the applying of thermal barrier coatings (TBC). Developing TBC systems and improving performance is an ongoing endeavour to prolong the lifetime. Thus, various studies have been conducted to find the optimum properties and dimensions. In this paper, the optimum thickness of intermediate bond coat (BC) and top coat (TC) have been determined via a novel hybrid particle swarm and simulated annealing stochastic optimization method. The optimum thicknesses have been achieved under the constraint of thermal stress induced by thermal fatigue, creep, and oxidation in the TC while minimizing the weight during twenty cycles. The solutions for BC and TC thicknesses are respectively 50 µm and 450 µm. Plane stress condition has been adopted for theoretical and finite element stress analysis, and the results are successfully compared.

Received on 13-06-2019
Accepted on 02-07-2019
Published on 14-10-2019

Keywords: Thermal barrier coating, Thickness, Optimization, PSO-SA, Thermal stress.

DOI: https://doi.org/10.6000/2369-3355.2019.06.01.1

1. INTRODUCTION

Increasing firing temperature of gas turbines for satisfying demands in energy supply and transportation systems menace hot section components of the engines like blades [1]. But applying thermal barrier coatings (TBC) has eliminated the problem by allowing the blade to operate at temperatures 100-300 °C lower than blade surface magnitude and maintaining the creep strength, as well as providing oxidation protection [2, 3]. A TBC system comprises a ceramic top coat (TC) as the insulator, a thermally grown oxide layer called TGO, and an intermediate metallic bond coat (BC). The TBC layers suffer different internal (e.g. creep, cracking, sintering, precipitation growth, etc.) and external (e.g. erosion, corrosion) deteriorating processes [4-9]. The unpredictability of the failure mechanisms and incomplete comprehension of the various phenomenon are unsafe obstacles to attain optimum performance of the TBC during service time. The optimal thickness of the TC and BC layers of the system is one of the ways to enhance the operation of the TBC by reducing the thermal stress while minimizing the overall weight.

Different studies have been conducted to design the most favourable TBC layers thickness. Li *et al*. [10] obtained a proper TBC thickness distribution by 3D finite element (FE) analysis and a subsequent weighted-sum approach to solve the optimization problem. They announced that insulation capability and thermal stress level are modified with TC thickness increase. Lim *et al*. [3] developed an FE model to calculate the TBC thermal stress considering the interaction of factors like oxidation and creep. A subsequent parametric study revealed that thermal stress is sensitive to material properties more than geometric parameters. Abedi *et al*. [11] examined the effect of different TC and BC thicknesses on microstructural, mechanical, and thermal shock characteristics of a triple layer TBC deposited on a carbon-fibre reinforced polyimide matrix composite. The authors reported that a TBC system with a 300 µm thick TC have clean and adhesive BC/substrate interface while cracks exist in the aforementioned zone of the TBC with a 400 µm TC

*Department of Electrical and Computer Engineering, University of Montreal, Concordia, Canada; E-mail: E-mail: ma.roudneshin@gmail.com

thickness. The existence of cracks will reduce the level of residual surface stress, too.

In contrast, an increase in TC thickness will boost thermal shock resistance. Moreover, among coated samples with 50, 100, and 150 μm thick BC layer, TBC system with 100 μm thick BC layer exhibited more significant qualities of adhesion strength and thermal shock resistance. Fang *et al*. [12] investigated the bonding strength of the BC/substrate interface and the oxidation rate of the TGO layer. Their observations revealed that the porosity level of the thin coating was smaller than that of the thick one and the pores are larger in the vicinity of the surface. Also, oxygen diffusion is influenced by thickening of the TC, which will further affect the oxidation rate.

In this paper, a Particle Swarm Optimization (PSO) - Simulated Annealing (SA) optimization method proposed by Javidrad and Nazari [13] is applied to find the optimum thickness of TC (t_{TC}) and BC (t_{BC}) layers of a TBC system to achieve the most desirable thermal stress. A planar stress formulation is implemented in the stress calculations [5]. The loading applied to the model includes thermal fatigue, creep, and oxidation. The optimization procedure conducted is a sample and is proposed as an applicable example that proves the applicability of PSO-SA optimization technique in multi-layer and multi-objective problems (not just theoretical disciplines). Besides, the paper means to find the optimal thicknesses of the TBC layers to reduce the thermal tensile stress provoked by temperature variation (thermal fatigue). The results were examined in comparison with the other similar paper [5] considering plasticity and temperature loss.

2. CALCULATION PROCEDURE

2.1. Analytical Stress Analysis

Plane-stress formulation is adopted in a four-layered axisymmetric solid disk since TBC system and substrate layer are thin in thickness (Figure **1**).

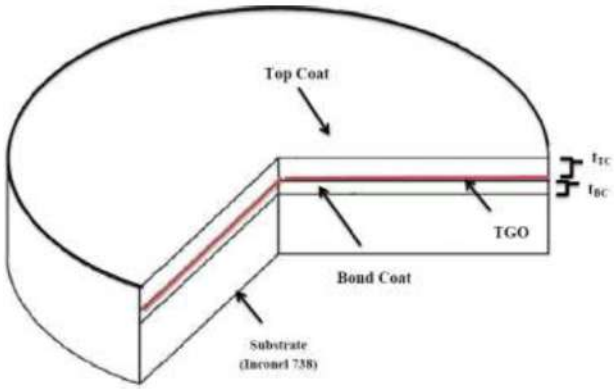

Figure 1: The four-layered disk as the axisymmetric model of the study.

By use of polar coordinate, the radial strain can be expressed by Hook's law as:

$$\varepsilon_r = \frac{1}{E}(\sigma_r - \nu\sigma_\theta) + \alpha\Delta T(t, th) \quad (1)$$

where ε_r, E, σ_r, ν, σ_θ, α, and ΔT are respectively the radial strain, module of elasticity, radial stress, Poisson's ratio, hoop stress, coefficient of thermal expansion and temperature change as a function of time (t) and thickness (th) (see section 2.2). Axisymmetry of the disk leads to equal radial and hoop components of stress and strain [4, 5, 14, 15]. So by considering thermal load and creep plasticity simultaneously, the radial stress of each layer can be rewritten as (subscripts dropped) [14]:

$$\sigma = \frac{E}{1-\upsilon}[\varepsilon - \alpha\Delta T + \varepsilon_{cr}] \quad (2)$$

Where ε_{cr} is creep strain and is stated by Norton power law as:

$$\varepsilon_{cr} = A\sigma^m t \quad (3)$$

Where A and m are constants reliant on material and t represents time (s). Norton law is applied in analytical modelling and FEM simulation together. Solving the radial force equilibrium equation of layers provides the ε parameter, as [14]:

$$\sum_{i=c,o,b,s} F = \sigma_i S_i = 0 \quad (4)$$

where S stands for the lateral area (disk base perimeter × disk height) and the subscripts c, o, b, and s symbolize the ceramic TC, TGO, BC, and substrate layers, respectively.

The TGO thickness growth is formulated by an exponential equation as [16]:

$$t_o = \left(A^o e - \frac{E_a}{RT}h\right)^n \quad (5)$$

Where t_o and h are respectively TGO thickness and hours of high-temperature exposure. Oxidation of the BC will thicken the TGO layer. I.e. it will increase the TGO height and hence is considered in S^o parameter in eq.4. The initial thickness of TGO is 1 μm [17].

Strain can be defined by deriving following equation through substitution of Eq. 2 into Eq. 4 and solving for ε:

$$\varepsilon = \varepsilon' = \frac{\left[\sum_{i=c,o,b,s}\left(\frac{E^i}{1-\nu^i}\alpha^i S^i\right)\right]\Delta T - \frac{E^i}{1-\nu^i}\varepsilon_i^{cr}}{\sum_{i=c,o,b,s}\left(\frac{E^i}{1-\nu^i}S^i\right)} \quad (6)$$

As creep strain depends on stress, the strain must be determined before stress calculation. Owing to short time increment during the calculation, in the first step, ε is obtained by excluding creep effect assuming quasi-static condition. Based on the calculated stress, creep strain can be

calculated, and the stress under thermal load and creep interaction (σ') is stated as [5]:

$$\sigma' = \frac{E}{1-\upsilon}\left[\varepsilon' - \alpha\Delta T\right] \tag{7}$$

It must be stated that interfacial roughness and associated out-of-plane stress of the TGO/TC interface has been neglected in the plane stress condition adopted in the paper. The roughness matters described above in analyzing the interfacial cracks, which is out of the scope of the paper. Besides, stress calculation is performed under the assumption of a stress-free state at room temperature.

2.2. Heat Transfer Analysis

On account of the temperature gradient across TBC layers, temperature non-uniformity is deliberated. Subsequently, the temperature distribution across the TBC system is determined by one-dimensional conduction Fourier's law as:

$$q = \frac{T_{sur}(t,th - T_{sub}(t,th)}{R} \tag{8}$$

where q, T_{sur}, and T_{sub} are respectively, heat flux [W/m^2], temperature on the surface of the coating, and temperature on the surface of the substrate both of which are functions of time (t) and thickness (L).

R =L/K stands for thermal resistance while K represents the thermal conductivity of each layer. Calculating total thermal resistance (R_{tot}) in eq.8 is needed for all three layers of the TBC in series sequence to find the T_{sub}.

$$R_{tot} = R_c + R_o + R_b \tag{9}$$

Where R_c, R_o, and R_b are respectively thermal resistance of ceramic TC, TGO, and BC (subscripts are the same as Eq. 4) (Figure **2**).

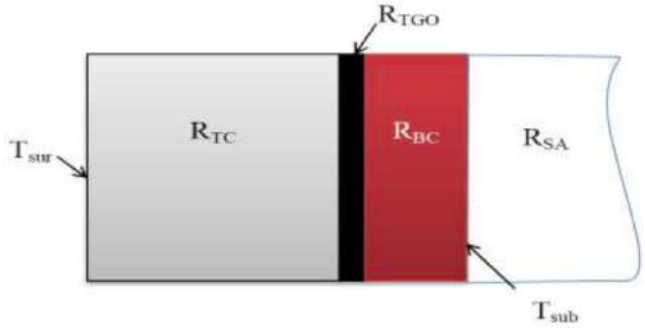

Figure 2: Schematic illustration of the heat transfer analysis of the one-dimensional conduction in TBC layers.

Temperature distribution in the TC (T_c), BC (T_b), and T_{sub} will be similarly calculated as (temperature of TC and TGO are assumed equal due to the small thickness of TGO):

$$T_c = T_{sur} - qR_c \tag{10-a}$$

$$T_b = T_{sur} - q(R_c + R_o) \tag{10-b}$$

$$T_{sub} = T_{sur} - q(R_c + R_o + R_b) \tag{10-c}$$

In the first step, eq. 8 is solved for the unoptimized TBC layers on the basis of the temperature values stated in the Koushali *et al*. [5] paper to find heat flux (q). Thereafter, eq.8 is reused to find the temperature distribution across the TBC layers for the same T_{sur}. The thermal cycle includes a 5-min heating, 45 min exposure at the peak temperature (T_{sur}=*1200°C*), and a cooling phase that lasts 5-min (Figure **3**).

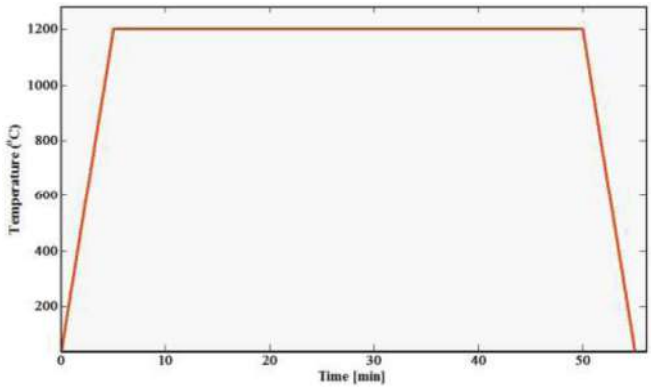

Figure 3: Temperature cycle imposed on the surface of the coating.

Heat transfer analysis is performed based on two conservative assumptions, both of which will result in the higher temperature of the substrate. Firstly, contact thermal resistance between layers is considered negligible [18]. Secondly, the substrate temperature right beneath the coating is assumed as the total temperature of the layer.

2.3. The Hybrid PSO-SA Algorithm/Programming Methodology

Before introducing the hybrid PSO-SA algorithm, it is worthwhile to explain each alone in advance. Particle swarm optimization is a population-based arbitrary search technique that is inspired by the social behaviour of birds and fishes. Consider a search space $S \in R^n$ of n dimensions and vector of design variables $D = \{D_1, D_2,..., D_n\}^T$.

Consider $D_k^i = \{D_1^i, D_2^i, ..., D_n^i\}^T$ as the position of particle k in iteration i, $P_k^b = \{P_1^b, P_2^b, ..., P_n^b\}^T$ as its best position in the search domain and $P^g=\{P_1^g, P_2^g, ..., P_n^g\}^T$ as the global best position visited by all particles, so far. At each iteration step i, the position and the velocity (movement vector) of the randomly distributed particles are updated successively according to the following equations [13, 19]:

$$v_k^{i+1} = \omega v_k^i + c_1 R_1 (P_k^b - D_k^i) + c_2 R_2 (P^g - D_k^i) \tag{11}$$

$$D_k^{i+1} = D_k^{i+1} + v_k^{i+1} \tag{12}$$

where v_k denotes the velocity of the kth particle, and R_1 and R_2 are random numbers between 0 and 1. c_1 and c_2 are two

controlling parameters called respectively cognitive parameter and social parameter. The calculated velocities of the particles are limited so as not to move beyond the interval [$-v_{max}$, v_{max}] where v_{max} is the maximum allowable velocity. The greater and smaller values of velocity are equal to v_{max} and $-v_{max}$, respectively. The function ω as a weighting factor is offered to achieve better control on the search scope. In other words, ω controls the exploration as a satisfactory movement of the particles crosswise the search space and also for exploitation prevention (localized search). One of the suggestions for ω is indicated as:

$$\omega = \omega_{max} - \left(\frac{\omega_{max} - \omega_{min}}{i_{max}} \right) \times i \quad (13)$$

Where i_{max} is the number of prescribed maximum iteration, and ω_{max} and ω_{min} are upper and lower limits of the weighting factor, respectively. Although PSO is known for its fast convergence, it may get stuck in local optima in multi-dimension problems following a fast convergence as an unreliable solution. Thus, in PSO, it is essential to balance between exploration and exploitation during the searching process for global convergence assurance.

A distinguishing characteristic of the SA algorithm is its integration with the Metropolis Monte Carlo procedure. In SA, the Metropolis procedure makes it possible that a state with a higher value be accepted with a probability, which is definitely the most important feature of the SA method [19].

The acceptance probability (P) of a candidate solution X_{i+1} from the current solution X_i is expressed as:

$$P = \begin{cases} 1, if\ f(D_{i+1}) \le f(D_i) \\ e^{-\Delta f/T}, \quad otherwise \end{cases} \quad (14)$$

Where f is the objective function, $\Delta f = f(D_{i+1}) - f(D_i)$, and T is a controlling parameter which is called temperature (by analogy). Successive temperature loss during the calculation results in acceptance probability reduction. Adequately high initial temperature together with a slow cooling rate, guarantee global optimum answer of SA. The most common temperature decrement rule follows as [19]:

$$T_{i+1} = R_T T_i \quad (15)$$

Where T_0 is the initial temperature, and R_T (cooling rate) is a positive constant usually taken in the range of 0.8–0.999.

The cost function of the study is the weight of the layers that is calculated by:

$$w = \sum_{i=c,o,b,s} \left(\rho^i V^i \right) \quad (16)$$

Where ρ and V respectively represent the density and volume of each layer (disk base area × disk height) and the subscripts c, o, b, and s are the same as Eq.4.

The hybrid PSO-SA algorithm benefits the individual positive features of each method by sequential application of both to not only assure convergence but also prevents the procedure from getting trapped into local solution. In other words, when PSO stopped, SA starts and replaces the global best result of PSO at that iteration (see Appendix) [13, 19].

The design variable of this study is thermal stress at the beginning of each thermal cycle. The optimization searches to find the optimal thermal stress less than the value resulted in the previous study of Koushali *et al*. [5]. This approach is performed by finding the optimal thickness of the TC and BC layer, in addition to minimizing the weight. After that, the resultant stress is verified by FE calculation and then optimized, and unoptimized stress values are compared.

2.4. Material Data

Excluding creep parameters, Poisson's ratio, and density, other material properties implemented in the modelling and simulation depend on the temperature within the range of 25-1200 °C and the selected values of them at 600 °C are presented in Table **1**. Poisson's ratio for the TC, TGO, BC, and the substrate is assumed 0.11, 0.24, 0.31, and 0.33 and their densities are 5650, 3978, 8100, and 8150 kg/m^3, respectively [20, 21].

Creep Norton law and TGO growth law constants are listed in Tables **2** and **3**, respectively. As the creep and oxidation processes are stimulated in the steady- temperature phase of thermal load, the parameters are temperature independent.

Table 1: Properties of the TBC and the Substrate at 600 °C [21, 22]

Property	TC	TGO	BC	Inconel 738
α (°×10^{-6}/°C)	10.1	8.7	15.2	16.2
E (GPa)	59	370	160	170
K (W/mK)	1.17	5.8	12	23.6
C (J/Kg°C)	450	980	620	690

Table 2: Norton Creep Parameters [20, 23, 24]

	TC	TGO	BC	Substrate	
Creep pre factor, A	2.25e-12		2.2e-12	7.3e-9	1.8e-8
Creep exponent, m	1	1	2.45	3	

Table 3: TGO Growth Law Parameters [16]

A^0	E_a	R	n
1.1338e-2	180,000	8.314	0.3225

2.5. FEM Model

A half TBC geometry is simulated owing to the axisymmetry of the disk which comprises four layers; the Nickel-based

Inconel 738 substrate, the BC layer (MCrAlY), the TGO layer, and the 8 wt% YSZ TC. The substrate and TGO initial thicknesses are 3200 μm and 0.5 μm, respectively. The disk radius (width of the model) is 1000 μm. A 2D mesh is produced with 1500 standard linear quadrilateral elements of the type coupled temp-displacement (CAX4T) provided by the FE tool ABAQUS (Figure **4**). Boundary conditions applied on the left, and the right sides are symmetry and periodicity, respectively. A multipoint constraint (MPC) of the type TIE allows the affected nodes of the right side to move simultaneously. Bottom edge nodes are horizontally permitted to displace through applying a vertical constraint while the top edge is free.

Isotropy and elastoplastic behaviour in addition to high-temperature creep, is supposed in all four layers. The swelling option is used in ABAQUS to model TGO growth behavior. Strain rate is equal to 7.5×10^{-18} and kept constant during the calculation. Additional details can be found in [25].

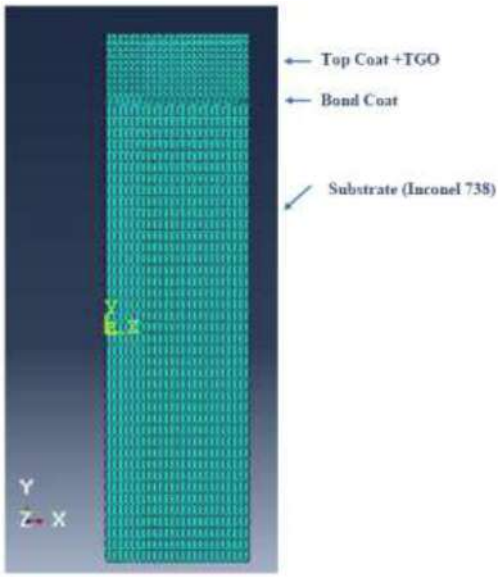

Figure 4: The meshing of the FE model composed of TBC and substrate layers.

3. RESULTS AND DISCUSSION

In the first step of the optimization procedure, the thickness range of two layers under consideration should be defined. Based on the works of literature, thickness range of BC and TC layers are 50-125 μm and 125-500 μm, respectively [17, 26]. PSO is the first method during the optimization procedure that starts with the creation of a population and introducing an initial temperature parameter. The temperature drops continuously after each cycle in PSO and each temperature equilibrium cycle (Markov chain loop) in SA according to a given cooling schedule. If the solution does not vary, it will be introduced to SA to search for a better position. The process mentioned above will endure until a valid result is achieved. The PSO population size, the initial temperature, the Markov chain length, R_T, c_1, and c_2 were set to 50, 1 and 100, 0.95, 2, and 2.2, respectively. The values mentioned above have been evaluated and successfully implemented in the optimization procedures for thirty benchmark functions [13, 19, 27].

Before starting the optimization procedure, the applied heat flux (q) on the surface of the coating must be determined. Heat flux is calculated by Eq. 8 for T_{sur}=1200°C, T_{sub} =960°C, TC's thickness of 150 μm and BC's thickness of 75 μm. As a result, the heat flux is 1.695 MW/m^2 that lies within the range assumed by Xue *et al*. [28]. Consequently, all the requisite parameters are known.

Based on the PSO-SA calculations, the optimal thicknesses found are respectively 50 μm and 450.5 μm for BC and TC layers. The calculated dimensions result in an overall weight of 0.0092mg and max stress of 23.5 MPa (Figures **5** and **6**). It can be seen that the results have converged in iteration 203 and kept constant after 1670 iterations.

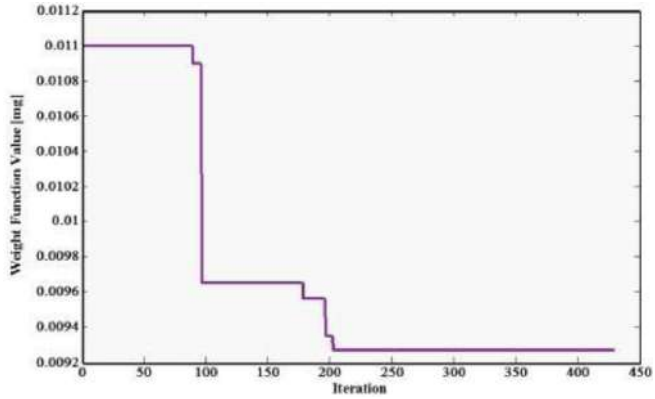

Figure 5: Convergence behaviour of the weight value of the total layers.

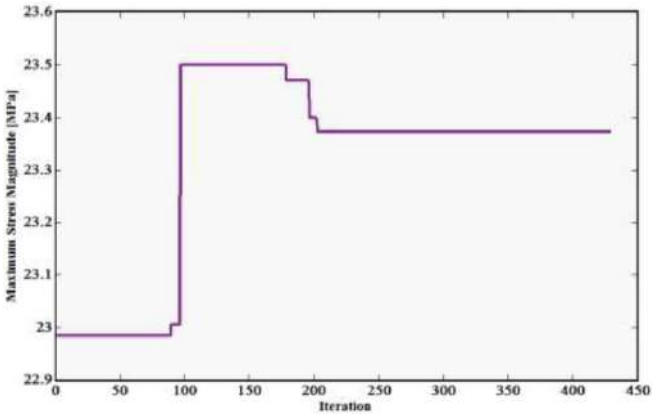

Figure 6: Convergence behaviour of the stress value of the TC.

Due to the metallic material of the BC layer; therefore, the highest density among three other layers of the TBC system, BC's thickness demonstrates no variation in the proposed range. Besides, the role of BC is to protect the substrate from oxidation, and it has no noteworthy impact in reducing temperature [26]. Thus, greater values for BC thickness won't

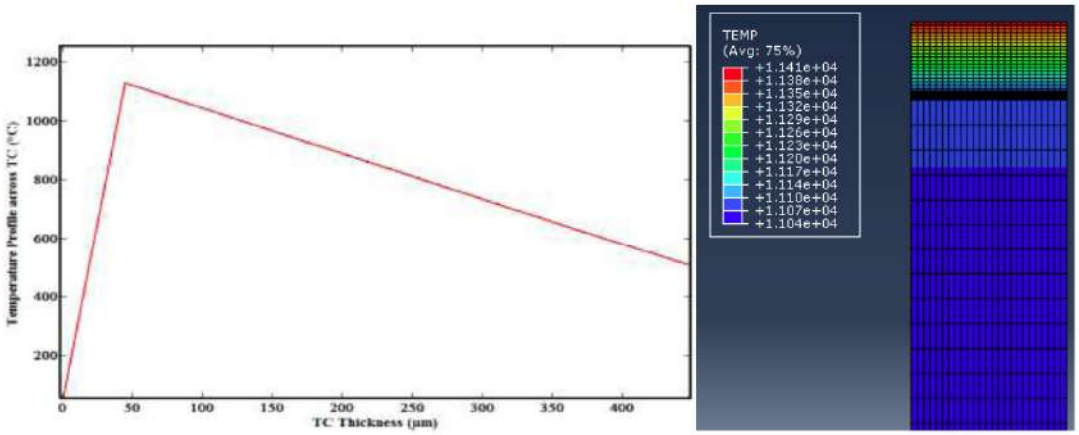

Figure 7: Analytical (a) and FE (b) solution of Temperature profile across TC during one cycle.

make sense. TC thickness can be varied as a result of several necessities. Thermal insulation role is mainly up to the top ceramic layer, thereby increasing the thickness will enhance this effect [29, 30]. Albeit this fact, the surplus thickness of the TC is not favourable because of chemical failure factors like sintering associated with high temperature. Besides, thickening TC will augment residual stress and strain, which is unsafe to TBC endurance by promoting interfacial delamination [31, 32]. The sensitivity of the top layer thickness to thermal stress is more pronounced rather than BC thickness [3]. Moreover, excessive weight is disadvantageous to the blade as a rotating component by intensifying the centrifugal force imposed [26].

T_{sub} for the optimized geometry with new layers' thicknesses equals to 500 °C and is 460 °C lower than the value assumed by Koushali *et al*. [5] attesting the insulative importance of the ceramic coating. Temperature profile across TC has been illustrated in Figure **7** in addition to the FE contour.

By definition of TBC layers dimensions and temperature distributions, details of analytical and FE calculations of stress variation of the TC layer during thermal load can be presented. In the first place, total strain variation (ε'-$\alpha\Delta T$) in eq.6 was calculated for the period of twenty cycles and is shown in Figure **8**.

The parameter ε' is constant through the TBC system and the layer underneath to satisfy the appropriate cohesion of layers. Solidity provision is the important reason of stress evolution in TC as a consequence of the difference in physical properties of layers (Table **1**). The descending attitude of strain during the dwell time of each cycle is attributed to the creep plastic deformation and subsequent stain energy release that puts the system in a lower energy level. The maximum magnitude of the total strain is 0.008 and decreases to - 0.051 by the end of the twentieth cycle. Accordingly, thermal stress can be calculated on the basis of strain value obtained, which exhibits the same trend as the strain behaviour (Figure **9**).

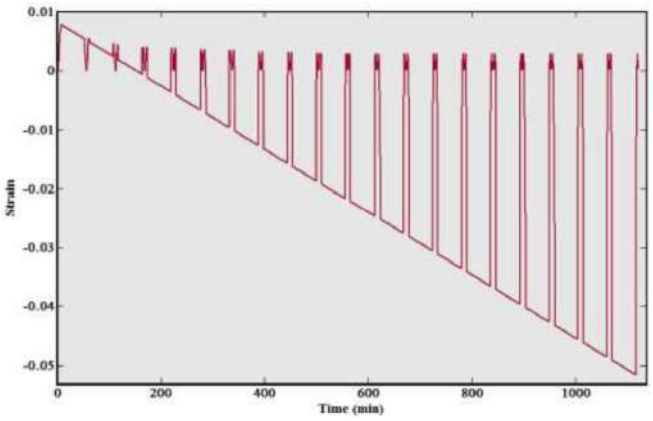

Figure 8: Strain variation of TC layer.

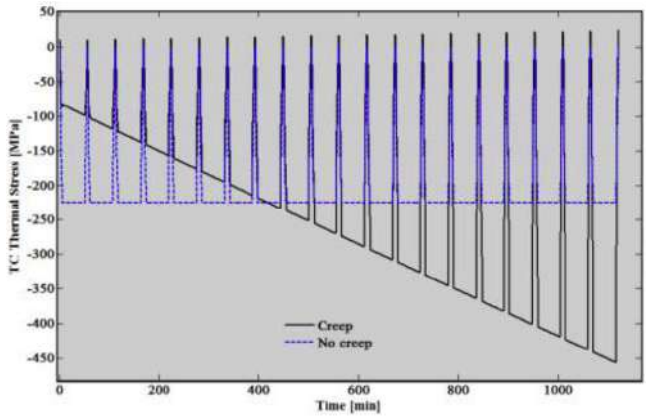

Figure 9: Stress Variation of TC layer.

If creep contribution neglected (dashed line in Figure **9**), compressive stress value of the TC during heating time is about 225 MPa. Conversely, the aforementioned value of the unoptimized system is +300 MPa [5]. The tensile stress has been altered to an expected compressive one due to the

temperature drop in the layers beneath TC that leads them to less expansion that will impose a tensile force on the hot TC. Moreover, a lower temperature will result in a lower coefficient of thermal expansion (α) as a temperature dependent property, hence lower αΔT (eq. 6).

Maximum tensile stress value occurs at the beginning of the heating phase at the last thermal cycle (23.5 MPa) and will be augmented due to the oxidation process and the thickening of the TGO layer.

Stress behaviour during the heating phase will continuously alleviate during the succeeding cycles, which is attributed to the energy release resulted by creep effect. Considering creep and thermal fatigue interaction, creep plasticity is the motive of stress relief, as stated in other studies [5, 20, 31].

As creep phenomena is dependent on stress, time, and temperature and will be activated when the temperature is high enough, stress demonstrates an ascending approach during variant temperature periods of heating and cooling. The cooling phase will hinder the creep process and leads to stress jump by the end of each cycle (thermal fatigue). At the end of the steady temperature phase of the last thermal cycle, stress magnitude is -455 MPa that agrees Zhao *et al*. [33] results.

Based on the optimization results that determine the optimal thickness of the TC and BC layers, FE geometry has been defined. Numerical FE simulation has been carried out to verify the analytical stress calculation of the optimized system. FE analytical solutions are depicted in Figure **10** that are in agreement. The plotted stress graph is of the elements near the surface, which experience higher temperature than the elements underneath.

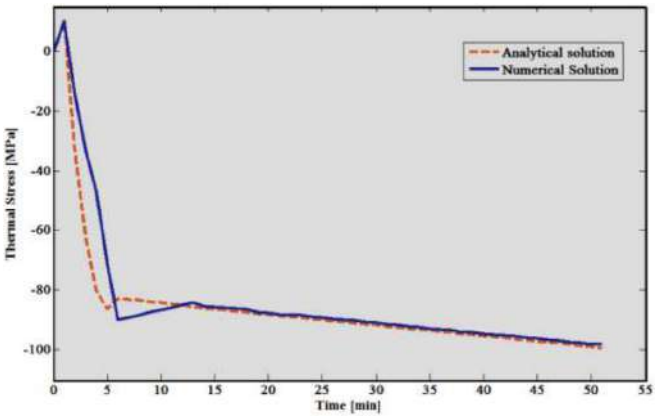

Figure 10: Analytical and FE solution of thermal stress in the first cycle.

Tighter boundary conditions are assigned to the left side of the model (symmetry constraint). I.e. rotational motion tangent to the symmetry plane must be equal to zero. Besides, no displacement happens in the normal direction. Hence, all nodal points along the line of symmetry are restrained against horizontal displacement. Consequently, left columns of the elements undergo more intense tension in comparison to the right and middle columns. Therefore, the diagram of Figure **10** is extracted from left side elements of the meshed geometry.

Creep analysis is performed through *Visco* step in ABAQUS. As ABAQUS cannot perform two steps at a time, a *Coupled temp-displacement* step was run for the heating phase of thermal loading, and *Visco* step was then activated.

The results of the optimized TBC system are compared to the previous work done by Koushali *et al*. [5]. The maximum positive stress values at the beginning of the heating steps of cycles (at the onset of creep activation) are of importance as they are destructive and will promote crack propagation. Reducing the value of this tensile stress is a significant accomplishment to enhance TBC life.

It is worth saying that excluding temperature drop influence and just taking into account the plasticity effect will also lead to a lower level of stress. I.e. the effect of thicker TC and thinner BC on strain variation (eq. 6) in comparison with unoptimized geometry. On the other hand, considering temperature drop instigated by thickening of TC will result in more stress alleviation. Hence, maximum stress magnitude during 20 cycles when temperature decline overlooked is 102 MPa. These tensile stresses calculated by current (with and without temperature effect) besides recent work [5] are demonstrated in the bar chart of Figure **11**.

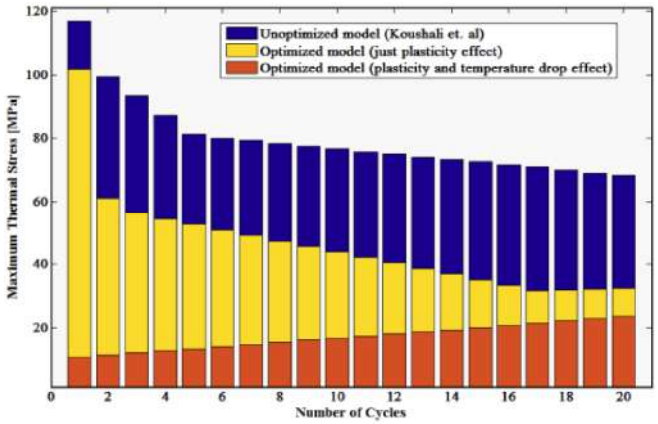

Figure 11: Comparison of maximum stress of twenty cycles calculated by two models.

When temperature decrease overlooked and just the plasticity effect considered (yellow bars of Figure **11**), the descending trend of stress that is attributed to creep plasticity is more intense in initial cycles. Meanwhile, as time passes, oxidation and subsequent thickening of the TGO layer adds extra load to the system and stress alleviation is not as remarkable as three initial cycles. The TGO growth rate is not constant at the primary fraction of the TBC service time and decreases until a steady state is reached [25]. However, creep plasticity is still dominant. The TGO layer final thickness is 2.2 μm. Contrarily, in case of considering

temperature drop as the consequence of thicker TC (orange bars of Figure **11**), more stress reduction is observed.

Moreover, unlike the case of considering plasticity individually, the max thermal stress demonstrates an ascending order, which is the result of substrate lower temperature. Therefore, cooler substrate resists against the expansion of the layers above. Since there is a thick substrate in the model in comparison to the TBC layers' thicknesses, the stiffness of the substrate surpasses the TBC layers and drives the deformation of the whole assembly. Furthermore, the lower temperature of the substrate reduces creep effect and makes the oxidation the dominant influential factor.

4. FINAL REMARKS

Thermal barrier coating (TBC) is being widely used to protect hot gas path components against different degrading factors during service life. Achieving the best performance of TBCs is of the high requirement by finding optimum dimensions in addition to optimal physical and mechanical properties. In this research, a hybrid coupled particle swarm and simulated annealing stochastic optimization (PSO-SA) method are introduced for finding the most favourable thickness of top and bond coat in the TBC system. The following conclusions are made:

1. The PSO-SA optimization technique practised in the calculations takes advantage of fast and secure convergence as the converged results were achieved within one second.

2. The solution reveals that a respectively 50 μm and 450 μm thick bond coat and top coat will result in optimal thermal stress while minimizing the weight.

3. A finite element stress analysis is performed to verify analytical stress calculation in the optimized TBC system, and two solutions are in agreement.

4. The loading consists of twenty thermal cycles, and the maximum stress of each cycle is compared to the unoptimized system. The solution validates the stress reduction achieved by layers thickness optimization. Considering temperature decline resulted by thicker ceramic TC will lead to further stress decrease.

APPENDIX

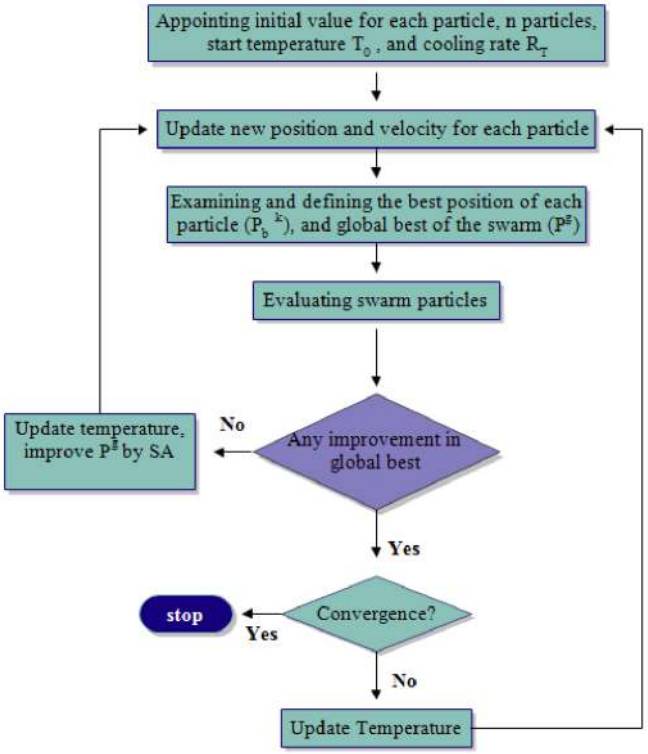

Figure A1: The procedure of the PSO-SA hybrid optimization method [19].

REFERENCES

[1] Cernuschi F, Lorenzoni L, Ahmaniemi S, Vuoristo P, Mäntylä T. Studies of the sintering kinetics of thick thermal barrier coatings by thermal diffusivity measurements. Journal of the European Ceramic Society 2005; 25(4): 393-400. https://doi.org/10.1016/j.jeurceramsoc.2004.01.009

[2] Osorio JD, Toro A, Hernandez-Ortiz JP. Thermal barrier coatings for gas turbine applications: failure mechanisms and key microstructural features. Dyna 2012; 79(176): 149-158.

[3] Lim JG, Seo S, Koo JM, Seok CS, Choi JB, Kim MK. Parametric study for optimal design of an air plasma sprayed thermal barrier coating system with respect to thermal stress. Surface and Coatings Technology 2017; 315: 105-111. https://doi.org/10.1016/j.surfcoat.2017.02.012

[4] Koushali AG, Sameezadeh M, Vaseghi M, Safarpour P. Analytical and numerical investigations of the crack behavior in thermal barrier coatings under the trip thermal load. Surface and Coatings Technology 2018; 337: 90-96. https://doi.org/10.1016/j.surfcoat.2018.01.010

[5] Koushali AG, Sameezadeh M, Vaseghi M, Safarpour P. Modeling and simulation of thermal fatigue crack in EB-PVD TBCs under non-uniform temperature. Ceramics International 2017; 43(16): 13140-13145. https://doi.org/10.1016/j.ceramint.2017.07.006

[6] Kumar V, Balasubramanian K. Progress update on failure mechanisms of advanced thermal barrier coatings: A review, Progress in Organic Coatings 2016; 90: 54-82. https://doi.org/10.1016/j.porgcoat.2015.09.019

[7] Naraparaju R, Hüttermann M, Schulz U, Mechnich P. Tailoring the EB-PVD columnar microstructure to mitigate the infiltration of CMAS in 7YSZ thermal barrier coatings. Journal of the European Ceramic Society 2017; 37(1): 261-270. https://doi.org/10.1016/j.jeurceramsoc.2016.07.027

[8] Lv B, Fan X, Li D, Wang T. Towards enhanced sintering resistance: Air-plasma-sprayed thermal barrier coating system with porosity gradient. Journal of the European Ceramic Society 2017. https://doi.org/10.1016/j.jeurceramsoc.2017.12.008

[9] Ozgurluk Y, Doleker KM, Karaoglanli AC. Hot corrosion behavior of YSZ, Gd2Zr2O7 and YSZ/Gd2Zr2O7 thermal barrier coatings exposed to molten sulfate and vanadate salt. Applied Surface Science 2017. https://doi.org/10.1016/j.apsusc.2017.09.047

[10] Li B, Fan X, Li D, Jiang P. Design of Thermal Barrier Coatings Thickness for Gas Turbine Blade Based on Finite Element Analysis. Mathematical Problems in Engineering 2017; 2017. https://doi.org/10.1155/2017/2147830

[11] Abedi H, Salehi M, Shafyei A. Microstructural, Mechanical and Thermal Shock Properties of Triple-layer TBCs with Different Thicknesses of Bond Coat and Ceramic Top Coat Deposited onto Polyimide Matrix Composite. Ceramics International 2018. https://doi.org/10.1016/j.ceramint.2018.01.006

[12] Fang X, Zhang G, Feng X. Performance of TBCs system due to the different thicknesses of top ceramic layer. Ceramics International 2015; 41(2): 2840-2846. https://doi.org/10.1016/j.ceramint.2014.10.105

[13] Javidrad F, Nazari M. A new hybrid particle swarm and simulated annealing stochastic optimization method. Applied Soft Computing 2017; 60: 634-654. https://doi.org/10.1016/j.asoc.2017.07.023

[14] Ali M, Nusier S, Newaz G. Creep effects on early damage initiation in a TBC system. Journal of Materials Science 2004; 39(10): 3383-3390. https://doi.org/10.1023/B:JMSC.0000026940.56103.d3

[15] Hetnarski RB, Eslami MR, Gladwell G. Thermal stresses: advanced theory and applications: Springer 2009.

[16] Asghari S, Salimi M. Finite element simulation of thermal barrier coating performance under thermal cycling. Surface and Coatings Technology 2010; 205(7): 2042-2050. https://doi.org/10.1016/j.surfcoat.2010.08.099

[17] Xu H, Guo H. Thermal barrier coatings: Elsevier 2011. https://doi.org/10.1533/9780857090829

[18] Liebert CH, Gaugler RE. The significance of thermal contact resistance in two-layer thermal-barrier-coated turbine vanes. Thin Solid Films 1980; 73(2): 471-475. https://doi.org/10.1016/0040-6090(80)90516-7

[19] Javidrad F, Nazari M, Javidrad H. Optimum stacking sequence design of laminates using a hybrid PSO-SA method. Composite Structures 2017. https://doi.org/10.1016/j.compstruct.2017.11.074

[20] Dong H, Yang G-J, Cai H-N, Ding H, Li C-X, Li C-J. The influence of temperature gradient across YSZ on thermal cyclic lifetime of plasma-sprayed thermal barrier coatings. Ceramics International 2015; 41(9): 11046-11056. https://doi.org/10.1016/j.ceramint.2015.05.049

[21] Mao W, Zhou Y, Yang L, Yu X. Modeling of residual stresses variation with thermal cycling in thermal barrier coatings. Mechanics of Materials 2006; 38(12): 1118-1127. https://doi.org/10.1016/j.mechmat.2006.01.002

[22] Busso EP, Qian Z, Taylor M, Evans H. The influence of bondcoat and topcoat mechanical properties on stress development in thermal barrier coating systems. Acta Materialia 2009; 57(8): 2349-2361. https://doi.org/10.1016/j.actamat.2009.01.017

[23] Bäker M. Finite element simulation of interface cracks in thermal barrier coatings. Computational Materials Science 2012; 64: 79-83. https://doi.org/10.1016/j.commatsci.2012.02.044

[24] Ranjbar-Far M, Absi J, Mariaux G, Smith D. Crack propagation modeling on the interfaces of thermal barrier coating system with different thickness of the oxide layer and different interface morphologies. Materials & Design 2011; 32(10): 4961-4969. https://doi.org/10.1016/j.matdes.2011.05.039

[25] Rösler J, Bäker M, Aufzug K. A parametric study of the stress state of thermal barrier coatings: Part I: creep relaxation. Acta Materialia 2004; 52(16): 4809-4817. https://doi.org/10.1016/j.actamat.2004.06.046

[26] Bose S. High temperature coatings: Butterworth-Heinemann, 2011.

[27] Norouzi S, Nazari M, Farahani MV. A Novel Hybrid Particle Swarm Optimization-Simulated Annealing Approach for CO2-Oil Minimum Miscibility Pressure (MMP) Prediction, in Proceeding of in Proceeding of 81st EAGE Conference and Exhibition, 2019.

[28] Xue Z, Evans A, Hutchinson J. Delamination Susceptibility of coatings under high thermal flux. Journal of Applied Mechanics 2009; 76(4): 041008. https://doi.org/10.1115/1.3086590

[29] Shao F, Zhao H, Zhong X, Zhuang Y, Cheng Z, Wang L, Tao S. Characteristics of thick columnar YSZ coatings fabricated by plasma spray-physical vapor deposition. Journal of the European Ceramic Society 2017. https://doi.org/10.1016/j.jeurceramsoc.2017.10.059

[30] Ma R, Cheng X, Ye W. SiC fiber and yttria-stabilized zirconia composite thick thermal barrier coatings fabricated by plasma spray. Applied Surface Science 2015; 357: 407-412. https://doi.org/10.1016/j.apsusc.2015.09.028

[31] Wang L, Li D, Yang J, Shao F, Zhong X, Zhao H, Yang K, Tao S, Wang Y. Modeling of thermal properties and failure of thermal barrier coatings with the use of finite element methods: A review. Journal of the European Ceramic Society 2016; 36(6): 1313-1331. https://doi.org/10.1016/j.jeurceramsoc.2015.12.038

[32] Fleck N, Cocks A, Lampenscherf S. Thermal shock resistance of air plasma sprayed thermal barrier coatings. Journal of the European Ceramic Society 2014; 34(11): 2687-2694. https://doi.org/10.1016/j.jeurceramsoc.2014.01.002

[33] Zhao X, Wang X, Xiao P. Sintering and failure behaviour of EB-PVD thermal barrier coating after isothermal treatment. Surface and Coatings Technology 2006; 200(20): 5946-5955. https://doi.org/10.1016/j.surfcoat.2005.09.006